Defect engineering of the electrochemical characteristics of carbon nanotube varieties

Mark A. Hoefer and Prabhakar R. Bandaru[a)]
Department of Mechanical and Aerospace Engineering, Materials Science Program, University of California, San Diego, La Jolla, California 92093-0411, USA

(Received 11 November 2009; accepted 29 May 2010; published online 5 August 2010)

The electrochemical behavior of carbon nanotubes (CNTs) containing both *intrinsic* and *extrinsically introduced* defects has been investigated through the study of bamboo and hollow multiwalled CNT morphologies. The controlled addition of argon ions was used for varying the charge and type of extrinsic defects. It was indicated from Raman spectroscopy and voltammetry that the electrocatalytic response of hollow type CNTs could be tailored more significantly, compared to bamboo type CNTs which have innately high reactive site densities and are less amenable to modification. An in-plane correlation length parameter was used to understand the variation of the defect density as a function of argon ion irradiation. The work has implications in the design of nanotube based chemical sensors, facilitated through the introduction of suitable reactive sites. © *2010 American Institute of Physics*. [doi:10.1063/1.3457227]

I. INTRODUCTION

The postulated fast electron transfer kinetics,[1] related to the large surface area/volume ratios, of carbon nanotubes (CNTs) could be useful for the development of increased sensitivity electrode materials, electrochemical sensors, supercapacitors, etc.[2–4] In this context, it has been pointed out that the electrocatalytic behavior along the length of the CNTs would be similar to the basal planes of graphite while the ends would correspond to the edge planes.[5,6] The latter corresponds to a large defect density, which could be profitably used for enhanced sensitivity. In this study, we investigate the influence of both intrinsic and extrinsic defects through a study of multiwalled, hollow-core CNTs (HCNTs) and bamboo-type CNTs (BCNTs). The HCNTs occur with sidewalls parallel to the nanotube axis—Fig. 1(a), while in the BCNT case, the morphology has periodic graphitic planes, angled away from the tube-axis, forming compartmentlike structures—Fig. 1(b). The hollow cores in HCNTs arise from the catalyst particle passivation at the center, while the prevention of passivation through using, e.g., NH_3, gives rise to BCNTs.[7,8] We show that argon ion exposure could be used to systematically tune the electrochemical behavior of both types of CNTs, through the introduction of additional defective sites with positive charge.

The degree of order in CNTs can be studied with Raman spectroscopy through the linear stretching of sp^2 bonds (E_{2g} mode), and is manifested through the intensity of the G-peak (frequency $\sim 1580\ cm^{-1}$). Noncollinear stretches due to defects, disorder, or the formation of adsorbates are evidenced through the D-peak,[9–12] at $\sim 1350\ cm^{-1}$ in the Raman spectra. Additionally, second order harmonic peaks in the range of $2500–3300\ cm^{-1}$ (e.g., $D^{(2)}/G' \sim 2700\ cm^{-1}$, $(D+G) \sim 2930\ cm^{-1}$) are more sensitive to structural changes in the CNTs (Ref. 10) and were also considered. The in-plane correlation length (L_a)—the size scale over which the CNT can be considered defect free, was used as a metric to quantify the degree of structural disorder and was obtained through a comparison of the D-and G-peak *intensity* ratio. For example, L_a is defined by the Tuinstra–Koenig relationship,[13,14] $L_a(\text{nm}) = 4.4/R$ where $R = (I_D/I_G)_L$. The peak widths [full width at half maximum (FWHM)] of the G-peaks (i.e., $\Delta\omega_G$) and D-peaks (i.e., $\Delta\omega_D$) are related to the spread of the energy distribution and were also considered.

Structural modification, through defects, could influence the predicted performance of CNTs for electrodes and was investigated through cyclic voltammetry (CV). For example, in a reversible one-electron transfer from the electrode to the redox couple [i.e., in $Fe(CN)_6^{3-} + e^- \leftrightarrow Fe(CN)_6^{4-}$] the cathodic peak current density (i_{pc}) is equal in magnitude to the anodic peak current density (i_{pa}). Nonideal electrode behavior, linked to irreversible electron transfer/adsorption processes[15] would be manifested through (i) a larger/smaller anode-cathode peak separation ($\Delta E_p = E_{pa} - E_{pc}$) compared to 59 mV (for a one-electron redox reaction, as above), and/or (ii) deviations in the $|i_{pc}/i_{pa}|$ ratio. Changes in the double-layer capacitance (C_{dl}), which arises due to charge separation

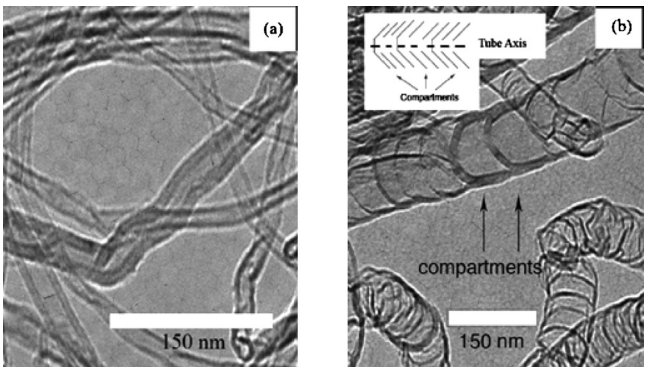

FIG. 1. Transmission electron microscopy images of CNTs of the (a) hollow (HCNT) and (b) bamboo (BCNT) morphology CNTs. The inset of (b) shows the orientation of the graphitic planes.

[a)]Electronic mail: pbandaru@ucsd.edu.

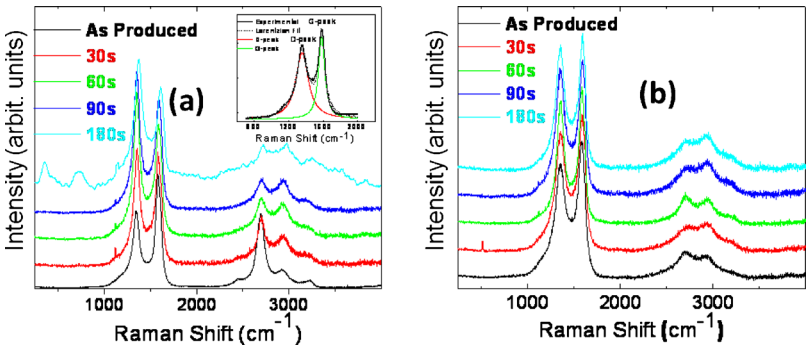

FIG. 2. (Color online) The Raman spectra for the as-produced and Ar exposed (a) BCNTs and (b) HCNTs, irradiated with argon for 30, 60, 90, and 180 s. The inset, in (a) illustrates Lorentzian peak fitting procedures for the D-(~1350 cm^{-1}) and G-peaks (~1580 cm^{-1}).

across the electrode/electrolyte interface, could also indicate changes in the charge density along the CNT.[2]

II. EXPERIMENTAL PROCEDURES

Both the hollow core (HCNTs, length 100 ± 5 μm, diameter 17 ± 3 nm) and bamboo (BCNTs, length 20 ± 2 μm, diameter 25 ± 5 nm) CNT morphologies were grown via thermal chemical vapor deposition on n-type Si substrates, using 5 nm thickness of Fe catalyst—deposited through electron-beam evaporation. The HCNTs were grown with a feed gas mixture composed of acetylene [5 SCCM (SCCM denotes cubic centimeter per minute at STP) for 1 min] and 200 SCCM argon at 615 °C. The BCNTs were grown[16] with feed gas composed of 100 SCCM of benzene, 500 SCCM argon, and 200 SCCM ammonia at 850 °C. Subsequently, for the purpose of introducing a controlled number of defects, the CNT samples were subject to argon irradiation in a reactive ion chamber. The influence of a large number of parameters, such as flow rate, irradiation time, power, and ambient pressure were probed. In this paper, a representative study is presented, where an argon flow rate ~10 SCCM, pressure ~30 mT, and power of 100 W was used with time scales in the range of 30–180 s.

Raman Spectroscopy (at 514.5 nm, 1.49 mW, with 90 s acquisition time) was then used for quantifying the degree of structural order and charge transfer characteristics,[11,16,17] in the untreated and argon irradiated samples. The electrochemical properties of the CNTs were subsequently investigated by placing them as working electrodes in CV experiments using a PCI4–300 potentiostat from Gamry Instruments Inc. A standard three electrode setup in a 1 M KCl supporting electrolyte solution containing various concentrations (1–10 mM) of $K_3Fe(CN)_6$, was employed with a (i) HCNT/BCNT *working electrode*, (ii) platinum wire *counter electrode*, and a (iii) saturated calomel *reference electrode*. We eliminated the possibility of hexacyanoferrate complex adsorbate formation on the electrodes[18] which could affect electrochemical kinetics, through the choice of the voltage scan range, of (−0.4)–0.8 V, and also through using freshly prepared (<2 h old) solutions.

III. RESULTS AND DISCUSSION

A. Probing the characteristics of irradiated HCNTs and BCNTs through Raman spectroscopy

As the CNTs are exposed to irradiation, the structural changes were represented by the changes in the first and second order G- and D-peak intensities (Fig. 2). Lorentzian fitting functions, for the intensity (I) of the form, $I = I_p(\Delta\omega)^2/4(f-f_c)^2+(\Delta\omega)^2$ were used[12,17,19] for extracting the peak position (f_c, in per centimeter), the peak height (I_p in counts), and $\Delta\omega$ (per centimeter). The results for HCNTs and BCNTs are presented in Tables I and II, respectively.

It was observed from the tables that even in the as-prepared form, the D-peak position for HCNTs (1347 cm^{-1}) was downshifted ~10 cm^{-1}, compared to the BCNTs (~1357 cm^{-1}) while the position of the G-peak (~1585 cm^{-1}) was similar. It was then surmised that the increased energy of the D-peak in BCNTs was probably due to the smaller equivalent crystallite sizes,[14] implicit in the bamboo morphology. Other manifestations of the greater disorder were seen through the larger G-peak width (~82 cm^{-1} for the BCNTs versus ~70 cm^{-1} for the HCNTs) along with a smaller L_a (~6.0 nm for the BCNTs versus 6.9 nm for the HCNTs).

With increasing argon exposure, the following were observed:

(a) a frequency upshift, along with larger disorder (represented through an increased $\Delta\omega_G$), of the G-peak. The disorder was relatively more for the HCNTs (increased

TABLE I. First order characteristics of HCNTs (in Raman spectroscopy), subject to increasing argon irradiation.

Ar irradiation time (s)	G-peak (cm^{-1})	D-peak (cm^{-1})	$(I_D/I_G)_L$	$\Delta\omega_G$ (cm^{-1})	$\Delta\omega_D$ (cm^{-1})	L_a (nm)
0	1586.4 ± 2.1	1347.0 ± 0.7	0.64 ± 0.02	70.0 ± 1.3	116.4 ± 7.5	6.9 ± 0.2
30	1586.0 ± 1.2	1353.0 ± 1.0	0.98 ± 0.08	89.5 ± 3.6	101.9 ± 2.0	4.5 ± 0.4
60	1587.4 ± 1.4	1353.0 ± 1.0	1.10 ± 0.03	89.2 ± 7.4	95.6 ± 7.2	4.0 ± 0.1
90	1588.2 ± 0.5	1353.6 ± 1.2	1.12 ± 0.04	89.3 ± 2.1	99.5 ± 0.5	3.9 ± 0.1
180	1590.2 ± 1.6	1353.8 ± 1.4	1.14 ± 0.07	89.5 ± 5.0	104.8 ± 8.0	3.9 ± 0.2

TABLE II. First order characteristics of BCNTs (in Raman spectroscopy), subject to increasing argon irradiation.

Ar irradiation time (s)	G-peak (cm^{-1})	D-peak (cm^{-1})	$(I_D/I_G)_L$	$\Delta\omega_G$ (cm^{-1})	$\Delta\omega_D$ (cm^{-1})	L_a (nm)
0	1584.6 ± 1.7	1356.7 ± 2.5	0.73 ± 0.05	82.1 ± 11.8	143.5 ± 41.6	6.0 ± 0.4
30	1587.8 ± 1.1	1359.4 ± 0.9	0.83 ± 0.01	92.6 ± 0.4	155.0 ± 3.9	5.3 ± 0.1
60	1588.0 ± 0.2	1358.0 ± 0.2	0.87 ± 0.03	85.7 ± 8.1	130.1 ± 27.7	5.1 ± 0.2
90	1589.4 ± 2.0	1356.6 ± 1.1	0.88 ± 0.04	90.2 ± 6.8	140.4 ± 17.6	5.0 ± 0.2
180	1591.3 ± 0.7	1356.8 ± 0.7	0.90 ± 0.00	90.9 ± 1.9	131.2 ± 2.8	4.9 ± 0.0

from ~70 to ~90 cm^{-1}) compared to the BCNTs (increased from ~82 to ~91 cm^{-1}).

(b) After initial exposure (i.e., argon for 30 s), the D-peak position and width was relatively unchanged for the HCNT, while it was similarly constant for the BCNTs.

(c) A larger increase in the intensity ratio, $(I_D/I_G)_L$, for the HCNTs compared to the BCNTs was also seen—Fig. 3.

(a) suggests that argon ions are being intercalated into the graphene planes forming acceptor-like defects. The higher G-peak frequencies, along with an increase in $\Delta\omega_G$, could be ascribed to a contraction of the intraplanar bond lengths, spanning a distribution of energies. While the G-peak position and $\Delta\omega_G$ for both HCNTs and BCNTs approach similar values with increased argon exposure (see Tables I and II), indicating a preponderance of defects, the former seem to be more amenable to defect introduction. While argon irradiation does appear to modulate the BCNT characteristics, the intrinsic defects—due to their morphology as depicted in Fig. 1(b), appear to dominate, as also indicated by the constancy of the D-peak from (b) and Table II.

The greater sensitivity of second order Raman peaks to both charge and defects was previously noted,[10] and is presented in Tables III and IV for HCNTs and BCNTs, respectively. For example, the G′ peak (the second harmonic of the D-peak, observable at ~2700 cm^{-1}) could be used to study localized charge transfer[20] where a frequency upshift would be indicative of acceptor-like doping. Indeed, from the tables, we observe such an increase for both HCNTs (from ~2694 to ~2705 cm^{-1}) and BCNTs (from ~2702 to ~2709 cm^{-1}). The sum harmonic (i.e., D+G) peak also indicated such a frequency upshift, for HCNTs (from ~2927 to ~2939 cm^{-1}) and BCNTs (from ~2933 to ~2939 cm^{-1}) which could follow from the first order G-peak dependence (Tables I and II). For the G′ peak, the FWHM of the untreated BCNTs, (i.e., $\Delta\omega_{G'} \sim 190$ cm^{-1}), was much larger than that of the untreated HCNTs, (i.e., $\Delta\omega_{G'} \sim 111$ cm^{-1}), implying greater localized disorder. However, on exposure to argon, there was a sudden jump in the linewidth for the BCNT G′-peak, from ~190 to ~293 cm^{-1}, which was relatively unchanged with further exposure, i.e., through a variation from ~293 to ~300 cm^{-1}, and which suggested a certain and small limit for argon incorporation. For the HCNTs there was a more gradual increase in the G′-peak FWHM from ~111 to ~138 cm^{-1}, implying gradual argon insertion. It was also seen that increasing irradiation decreases the peak intensity, and implies diminishing second order phonon processes.[21,22]

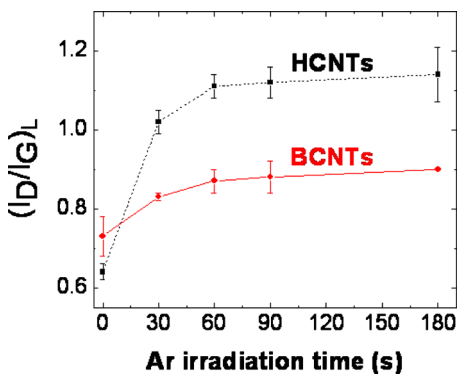

FIG. 3. (Color online) The variation in the line intensity ratio $(I_D/I_G)_L$ for the HCNTs (black squares) and BCNTs (red diamonds), indicates that the former are more amenable to modification.

In summary, the original defect density seems to dictate the degree to which the nanotubes could be tailored through argon exposure. BCNTs with a structural morphology implying a high intrinsic defect density were less amenable to subsequent structural and charge modification, compared to HCNTs.

B. Characterization of HCNTs and BCNTs through CV

The cyclic voltammograms for the HCNT and BCNT samples are shown in Fig. 4, and the accrued information summarized in Tables V and VI, respectively. In the CV characterization, it was observed that the $|i_{pc}/i_{pa}|$ ratio was approximately unity for both varieties of nanotubes. However, an increase in both i_{pc} and i_{pa}, of ~70%, e.g., an increase in i_{pc} from ~1.6 to 2.7 $\mu A/cm^2$, was noted for the HCNTs (Table V) while the BCNT peak current densities exhibit a much smaller range of variation of ~25% with increased argon irradiation time. The increase in the current density (i_{pa} and i_{pc}) could arise from the availability of additional reactive sites/defect density, due to argon irradiation. A larger peak current density in the BCNTs (Table VI), compared to HCNTs (Table V) could be correlated with a larger intrinsic defect density in the former. The change in the electrochemical characteristics could be indicated through the deviation of the ΔE_p (anode-cathode peak potential separation) from the ideal value of 59 mV, as well. It was seen that the initial ΔE_p for HCNTs was ~63 mV and for the BCNTs ~46 mV. With increased argon exposure, the ΔE_p exhibited a much larger variation for the HCNTs (increasing by ~90%, from ~63 to ~118 mV) compared to the BCNTs

TABLE III. Second order characteristics of HCNTs (in Raman spectroscopy), subject to increasing argon irradiation.

Ar irradiation time (s)	G′		D+G	
	G′ -peak (cm^{-1})	$\Delta\omega_{G'}$ (cm^{-1})	D+G-peak (cm^{-1})	$\Delta\omega_{(D+G)}$ (cm^{-1})
0	2693.8 ± 1.1	111.2 ± 19.9	2927.4 ± 4.1	200.3 ± 30.9
30	2698.8 ± 1.2	108.6 ± 4.8	2931.0 ± 4.0	238.8 ± 13.5
60	2702.8 ± 2.4	129.8 ± 19.3	2933.5 ± 2.5	218.0 ± 15.5
90	2703.2 ± 1.6	145.2 ± 5.9	2932.7 ± 1.3	232.4 ± 25.1
180	2704.9 ± 1.4	138.28 ± 11.8	2938.9 ± 6.6	288.6 ± 98.6

TABLE IV. Second order characteristics of BCNTs (in Raman spectroscopy), subject to increasing argon irradiation.

Ar irradiation time (s)	G′		D+G	
	G′ -peak (cm^{-1})	$\Delta\omega_{G'}$ (cm^{-1})	D+G -peak (cm^{-1})	$\Delta\omega_{(D+G)}$ (cm^{-1})
0	2702.3 ± 4.8	190.0 ± 57.8	2932.7 ± 1.0	223.5 ± 8.9
30	2712.0 ± 1.1	292.7 ± 10.2	2939.1 ± 1.2	254.7 ± 6.2
60	2708.2 ± 3.3	227.2 ± 84.2	2938.5 ± 0.5	230.9 ± 21.1
90	2712.5 ± 5.3	298.9 ± 25.2	2939.8 ± 2.2	228.2 ± 13.4
180	2708.9 ± 3.6	299.8 ± 44.3	2938.6 ± 1.2	229.1 ± 12.4

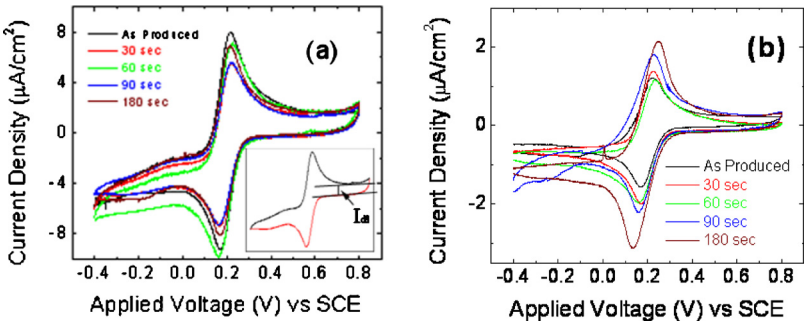

FIG. 4. (Color online) Cyclic voltammograms for (a) BCNTs and (b) HCNTs as a function of increased argon irradiation. The inset in (a) indicates the procedure through which the double-layer current, I_{dl}, was obtained from a given voltammogram. A scan rate of 20 mV/s with a 3 mM $K_3Fe(CN)_6$ was used.

TABLE V. Characteristics of HCNTs obtained through CV, subject to increasing argon irradiation, where v =20 mV/s and $[K_3Fe(CN)_6]$=3 mM.

Ar irradiation time (s)	i_{pc} ($\mu A/cm^2$)	i_{pa} ($\mu A/cm^2$)	$\lvert i_{pc}/i_{pa}\rvert$	ΔE_p (mV)	C_{dl} ($\mu F/cm^2$)	d (nm)
0	1.6 ± 0.3	−1.5 ± 0.0	1.1 ± 0.3	62.5 ± 2.1	7.2 ± 0.4	9.3
30	1.6 ± 0.2	−1.6 ± 0.2	1.0 ± 0.1	51.0 ± 3.0	10.4 ± 0.2	6.7
60	1.7 ± 0.4	−1.7 ± 0.4	1.0 ± 0.1	71.3 ± 8.9	12.5 ± 2.4	5.6
90	2.1 ± 0.3	−1.8 ± 0.3	1.2 ± 0.1	81.0 ± 5.5	16.1 ± 0.5	4.3
180	2.7 ± 0.3	−2.5 ± 0.9	1.1 ± 0.0	118.0 ± 8.4	28.3 ± 2.5	2.5

TABLE VI. Characteristics of BCNTs obtained through CV, subject to increasing argon irradiation, where v =20 mV/s and $[K_3Fe(CN)_6]$=3 mM.

Ar irradiation time (s)	i_{pc} ($\mu A/cm^2$)	i_{pa} ($\mu A/cm^2$)	$\lvert i_{pc}/i_{pa}\rvert$	ΔE_p (mV)	C_{dl} ($\mu F/cm^2$)	d (nm)
0	8.9 ± 0.6	−8.8 ± 1.0	1.0 ± 0.2	45.5 ± 0.7	87.0 ± 4.0	0.9
30	7.1 ± 1.1	−6.9 ± 1.0	1.0 ± 0.1	58.6 ± 5.6	54.8 ± 6.6	1.3
60	8.5 ± 0.3	−8.6 ± 1.0	1.0 ± 0.2	65.7 ± 2.1	59.5 ± 8.8	1.2
90	6.5 ± 0.3	−6.6 ± 0.4	1.1 ± 0.1	59.5 ± 2.1	61.8 ± 2.8	1.1
180	7.7 ± 1.2	−7.7 ± 1.1	1.1 ± 0.3	64.9 ± 1.0	75.9 ± 9.2	1.0

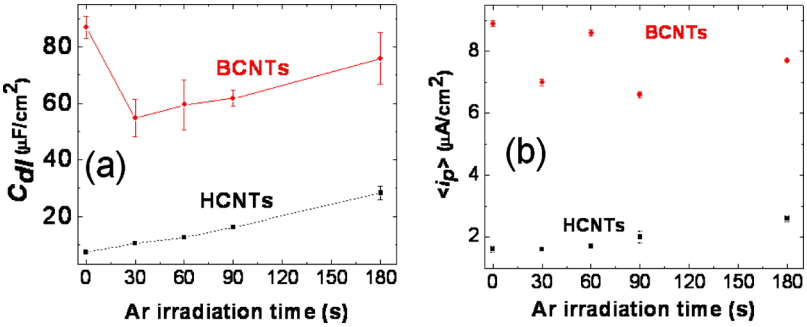

FIG. 5. (Color online) The variation in the (a) double-layer capacitance, C_{dl} and (b) the averaged peak current density, $\langle i_p \rangle$, with argon irradiation time for the HCNTs (black squares) and BCNTs (red diamonds).

(which increases by ~40%, from 46 to 65 mV). ΔE_p values lower than 59 mV could presumably be due to the adsorption of electroactive species onto the CNT electrode,[15] i.e., as $\Delta E_p = 0$ mV for adsorbed species (if the oxidized and reduced forms adsorb with the same affinity),[23] a contribution from both adsorbates and species in solution would lead to values intermediate between 0 and 59 mV.

Consequently, both argon irradiated HCNTs and BCNTs indicate quasireversible electron transfer kinetics, with a greater influence manifested in the HCNTs.[15,20] Such diminished kinetics could arise from an increased density of species surrounding the CNTs and may be brought about by the enhanced number of defects. The ΔE_p may also increase due to the increased activation energy, intrinsic to the defective sites induced by irradiation, for the occurrence of electrochemical reactions. An additional metric could then be the value of the double-layer capacitance (C_{dl}) which denotes the change in the CNT electrode characteristics as a function of argon irradiation. In this case, an increased defect density could presumably result in larger capacitance values. We calculated C_{dl} from the double-layer current I_{dl} ($=\upsilon\ C_{dl}$), at a given scan rate, υ (in millivolt per second). I_{dl} was determined from the cyclic voltammogram using procedures outlined in Bard and Faulkner,[15] and indicated in the inset to Fig. 4(a). We used a simple approximation, using the Helmholtz model,[23] for $C_{dl}(=\varepsilon\varepsilon_0 A/d)$, modeling the capacitance as due to a double layer of thickness, d, with A as the electrode area, ε the dielectric permittivity of the surrounding solution (~80), and ε_0 being the permittivity of free space ($=8.854\times10^{-12}$ C^2/Nm^2). It is noted that as the volume ratio of KCl to water is ~1:24, an estimate of ~80 for ε is reasonable. Additional considerations,[24] incorporating polarizability and hydration effects also yield a variability of ε of at most ~10%. This in turn implies an equivalent error in the estimation of the C_{dl} and is close to the experimental error, as indicated in Tables V and VI.

Generally, the Helmholtz model is quite simplistic compared to other models such as the Stern model or the more advanced electrochemical models.[23] However, the net capacitance is determined by the parallel combination of the fixed double layer, diffuse layer, solvent layer, etc. As we operate at values of applied potential larger than that corresponding to the point of zero charge, it could be a reasonable estimate to consider the capacitance due to the fixed double layer alone, as is assumed in the model. While we have observed a dependence of the capacitance on the concentration (which is again not considered in the Helmholtz model), in this paper we analyze results at a particular value of the concentration, i.e., 3 mM (as in Tables V and VI) for which our modeling might be adequate.

The area of the CNT electrode was approximated to be ~110 m^2/g and ~75 m^2/g for HCNTs and BCNTs, respectively, through considering the total surface area of the nanotubes,[25] treating each CNT as an individual electrode. Generally, in the use of CNTs as electrodes, one can consider two possibilities, i.e., corresponding to the cases where (1) each CNT acts as an independent electrode or (2) the individual diffusion layers of each CNT overlap resulting in a macroelectrodelike behavior. In case (1), the effective area could be estimated by considering the CNTs to be cylindrical with an average surface area of $2\pi rh$, where r is the nanotube radius and h is the nanotube height, and multiplying by the total number of CNTs on the Si substrate (estimated from an average spacing between the grown CNTs and the length and width of the Si substrate). This results in a total electrode area of the order of 10 cm^2. In case (2), the projected area of the substrate is considered and yields a total area of the order of 0.05 cm^2 (say, corresponding to a 7×7 mm^2 substrate).

When the value of the d, corresponding to cases (1) and (2) is estimated from the C_{dl}, for the latter case we seem to obtain unrealistic d values of the order of ~0.006 nm! Even if it is assumed that the ions are intimately adsorbed to the CNT surface, the ΔE_p should be ~0, which was not seen. The results of the computed C_{dl} for HCNTs and BCNTs subject to argon exposure are indicated in Tables V and VI, respectively, and are plotted in Fig. 5(a). It was seen that, C_{dl} of the HCNTs increases (~300%) with increased argon irradiation, along with a concomitant increase in the magnitude of E_{pa}, E_{pc}, and hence ΔE_p, while the C_{dl} of the BCNTs remains relatively constant. Contrary to HCNTs, intrinsic defects and morphology seem to dominate over the influence of those defects generated through argon exposure in BCNTs.

IV. CONCLUSIONS

We have shown that exposure to argon irradiation, through the controlled incorporation of defects, can influence the charge state of both *bamboo* and *hollow* variety CNT morphologies. Raman spectroscopy analysis, through the peak shifts and broadening, indicated nanotube charging and passivation. It is plausible that argon, through intercalation in the CNTs, abstracts electrons creating acceptor like defects. It was also concluded that the initial structural state could limit the relative amount of charge and defects that could be introduced. Consequently, BCNTs seem to be inherently better, compared to HCNTs, for electrodes in electrochemical processes due to larger intrinsic defect density. However, HCNTs allow for a greater degree of tunability and a range of electron transfer kinetics, made possible through argon irradiation. While the peak potential difference, ΔE_p, was seen to increase for both BCNTs and HCNTs due to argon exposure, the peak current ratio $|i_{pc}/i_{pa}|$, remained close to unity indicating quasireversible kinetics. Our work contributes to a better understanding of defects in CNTs and could be applied for tuning the electrochemical properties of CNT based electrodes, e.g., in chemical sensors and capacitors.

ACKNOWLEDGMENTS

We gratefully acknowledge support from the National Science Foundation (Grant No. ECS-05-08514) and the Office of Naval Research (Award No. N00014-06-1-0234). We thank Professor Frank Talke's group at the Center for Magnetic Recording Research (CMRR) at UC, San Diego for help with the Raman spectroscopy.

[1] J. M. Nugent, K. S. V. Santhanam, A. Rubio, and P. M. Ajayan, Nano Lett. **1**, 87 (2001).
[2] M. Hoefer and P. R. Bandaru, Appl. Phys. Lett. **95**, 183108 (2009).
[3] R. H. Baughman, A. A. Zakhidov, and W. A. de Heer, Science **297**, 787

(2002).
[4]Q. Zhao, Z. Gan, and Q. Zhuang, Electroanalysis **14**, 1609 (2002).
[5]C. E. Banks, R. R. Moore, T. J. Davies, and R. G. Compton, Chem. Commun. (Cambridge) **16**, 1804 (2004).
[6]C. E. Banks, T. J. Davies, G. G. Wildgoose, and R. G. Compton, Chem. Commun. (Cambridge), 829 (2005).
[7]F. Ding, K. Bolton, and A. Rosen, J. Electron. Mater. **35**, 207 (2006).
[8]C. H. Lin, H. L. Chang, C. M. Hsu, A. Y. Lo, and C. T. Kuo, Diamond Relat. Mater. **12**, 1851 (2003).
[9]T. C. Chieu, M. S. Dresselhaus, and M. Endo, Phys. Rev. B **26**, 5867 (1982).
[10]M. S. Dresselhaus, G. Dresselhaus, A. Jorio, A. G. Souza Filho, and R. Saito, Carbon **40**, 2043 (2002).
[11]M. S. Dresselhaus, G. Dresselhaus, M. A. Pimenta, and P. C. Eklund, in *Analytical Applications of Raman Spectroscopy*, edited by M. J. Pelletier (Blackwell Science, Malden, 1999), pp. 367–434.
[12]B. S. Elman, M. S. Dresselhaus, G. Dresselhaus, E. W. Maby, and H. Mazurek, Phys. Rev. B **24**, 1027 (1981).
[13]D. S. Knight and W. B. White, J. Mater. Res. **4**, 385 (1989).
[14]F. Tuinstra and J. L. Koenig, J. Chem. Phys. **53**, 1126 (1970).
[15]A. J. Bard and L. R. Faulkner, *Electrochemical Methods: Fundamentals and Applications*, 2nd ed. (Wiley, New York, 2001).
[16]B. S. Elman, M. S. Dresselhaus, M. Shayegan, H. Mazurek, and G. Dresselhaus, Phys. Rev. B **25**, 4142 (1982).
[17]J. Robertson, Mater. Sci. Eng. R. **37**, 129 (2002).
[18]C. M. Pharr and P. R. Griffiths, Anal. Chem. **69**, 4673 (1997).
[19]E. F. Antunes, A. O. Lobo, E. J. Corat, V. J. Trava-Airoldi, A. A. Martin, and C. Verissimo, Carbon **44**, 2202 (2006).
[20]K. McGuire, N. Gothard, P. L. Gai, M. S. Dresselhaus, G. U. Sumanasekera, and A. M. Rao, Carbon **43**, 219 (2005).
[21]A. C. Ferrari and J. Robertson, Phys. Rev. B **61**, 14095 (2000).
[22]P. C. Eklund, J. M. Holden, and R. A. Jishi, Carbon **33**, 959 (1995).
[23]C. M. A. Brett and A. M. O. Brett, *Electrochemistry: Principles, Methods, and Applications* (Oxford University Press, Oxford, 1993).
[24]K. Nörtemann, J. Hilland, and U. Kaatze, J. Phys. Chem. A **101**, 6864 (1997).
[25]A. Peigney, C. Laurent, E. Flahaut, R. R. Basca, and A. Rousset, Carbon **39**, 507 (2001).